JOURNAL OF Applied Polymer SCIENCE

Preparation and Characterization of Nanohydroxyapatite Strengthening Nanofibrous Poly(L-Lactide) Scaffold for Bone Tissue Engineering

Wanqing Han,[1] Jianhao Zhao,[1,2] Mei Tu,[1,2] Rong Zeng,[1,2] Zhengang Zha,[3] Changren Zhou[1,2]

[1]Department of Material Science and Engineering, College of Science and Engineering, Jinan University, Guangzhou 510632, China

[2]Department of Research and Development, Engineering Research Center of Artificial Organs and Materials, Ministry of Education, Guangzhou 510632, China

[3]Department of Orthopedics, First Hospital Attached to Jinan University, Guangzhou 510632, China

Correspondence to: J. Zhao (E-mail: jhzhao@jnu.edu.cn)

ABSTRACT: A biomimetic nanofibrous poly(L-lactide) scaffold strengthened by nanohydroxyapatite particles was fabricated via a thermally induced phase separation technique. Scanning electron microscopy results showed that nanohydroxyapatite particles uniformly dispersed in the nanofibrous poly(L-lactide) scaffold (50–500 nm in fiber diameter) with slight aggregation at a high nHA content, but showed no influence on the interconnected macroporous and nanofibrous structure of the scaffold. The nanofibrous poly(L-lactide) scaffold presented a specific surface area of 34.06 $m^2\ g^{-1}$, which was much higher than that of 2.79 $m^2\ g^{-1}$ for the poly(L-lactide) scaffold with platelet structure. Moreover, the specific surface area of the nanofibrous scaffold was further enhanced by incorporating nanohydroxyapatite particles. With increasing the nanohydroxyapatite content, the compressive modulus and amount of bovine serum albumin adsorbed on the surface of the nanofibrous composite scaffold were markedly improved, as opposed to the decreased crystallinity. In comparison to poly(L-lactide) scaffold, both the nanofibrous poly(L-lactide) and poly(L-lactide)/nanohydroxyapatite scaffolds exhibited a faster degradation rate for their much larger specific surface area. The culture of bone mesenchymal stem cell indicated that the composite nanofibrous poly(L-lactide) scaffold with 50 wt % nanohydroxyapatite showed the highest cells viability among various poly(L-lactide)-based scaffolds. The strengthened biomimetic nanofibrous poly(L-lactide)/nanohydroxyapatite composite scaffold will be a potential candidate for bone tissue engineering. © 2012 Wiley Periodicals, Inc. J. Appl. Polym. Sci. 000: 000–000, 2012

KEYWORDS: biomimetic; fibers; nanoparticles; phase separation; polyesters

Received 27 December 2011; accepted 7 June 2012; published online
DOI: 10.1002/app.38177

INTRODUCTION

In tissue engineering, scaffolds are constructed to serve as a temporary artificial extracellular matrix (ECM) for the purpose of supporting cell adhesion and promoting three-dimensional (3D) tissue formation.[1–3] The strategy for such scaffolds has recently focused on the construction of nanofibrous scaffolds that mimicked the structure of fibrillar collagen (50–500 nm in diameter), which abundantly existed in nature ECM.[4–6] As to the fabrication of nanofibrous scaffolds, three technologies including electrospinning, self-assembly and phase separation have been well developed.[7] Previous research showed that thermally induced phase separation (TIPS) would be a promising technique for it can not only produce nanofibers with controlled nanoscale size, but also combine with other techniques, such as particle leaching, to construct the desired 3D interconnected porous nanofibrous scaffolds, which is in favor of the transport of nutrient and cell metabolites.[8]

Poly(L-lactide) (PLLA), a class of synthetic polyester, has been widely applied in biomedical field for its favorable biodegradability and biocompatibility.[9–11] It has been recently found that nanofibrous structure mimicking the collagen nanofiber network in the natural ECM could facilitate cell growth and differentiation, such that various PLLA-based nanofibrous scaffold have been developed for bone tissue engineering.[12,13] However, nanofibrous PLLA (NF-PLLA) scaffold with high porosity and interconnected macroporous structure typically exhibited poor mechanical property that limited its application in bone tissue regeneration.[14] As we know, most of the previous literatures have mainly highlighted the effect of nanofibrous structure of

NF-PLLA scaffolds on the cell behavior, and few works have been investigated on the improvement of mechanical property of NF-PLLA scaffolds.[15] As a scaffold for bone tissue engineering, the basic requirement is to possess good mechanical property for supporting cell growth and new tissue formation. Generally, a common method for improving the strength of polymers is to blend with nanoscale particles or fibers.[16] Hydroxyapatite (HA), possessing the same composition and similar structure to the inorganic component of nature bone, could react with physiological fluids to form tenacious bonds with hard tissue,[17] hence presents superior bioactivity and osteoinductive property. Nevertheless, due to the brittleness and difficulty to process into complex shapes, HA is rarely to be utilized alone and thus is often used as a blending composition in the fabrication of tissue engineering scaffold.[18] Blending with nanohydroxyapatite (nHA) in high content and investigating the influence of nHA on the structure and properties of NF-PLLA scaffolds have been little concerned.

In this work, biomimetic 3D porous NF-PLLA scaffolds strengthened with different contents of nHA (NF-PLLA/nHA) were fabricated by a liquid–liquid TIPS technique using paraffin microspheres as porogens. The morphology, specific surface area, compressive properties, thermal properties, *in vitro* degradation, protein adsorption, and cell compatibility of NF-PLLA/nHA scaffolds were evaluated. As comparison, PLLA and NF-PLLA scaffolds without nHA were also prepared.

MATERIALS AND METHODS

Materials

Poly(L-lactide) (PLLA) (M_w = 400 kDa) was purchased from Shandong Institute of Medical Instruments. Nanohydroxyapatite (nHA) with a particle size of 55–60 nm[19] was provided by Biomaterials Research Institute, South China University of Technology. Bovine serum albumin (BSA) was purchased from Dingguo Bioengineering, Beijing, China. All other reagents and solvents used were analytical grade.

Fabrication of PLLA-based Scaffold

For the fabrication of NF-PLLA scaffold, paraffin spheres with a diameter of 300–450 μm, were used as porogens. About 4% (w/v) PLLA/dioxane/pyridine (1 : 1, v/v) homogeneous solution was dropped to entirely fill a paraffin sphere assembled template, which was previously heated at 37°C for 40 min. The complex was induced to liquid–liquid phase separation at −80°C for 6 h and then soaked in cold hexane (−18°C) to remove the paraffin and solvent.[20] The NF-PLLA scaffold was obtained after a further immersion in hexane and cyclohexane in sequence, followed by lyophilization (0.5 mmHg) at −80°C for 48 h.

NF-PLLA/nHA composite scaffolds with various nHA contents were constructed by the same process above except with the homogenous mixture of PLLA solution and nHA particles instead of PLLA solution. The nanofibrous composite scaffolds with a weight percentage of 30, 50, and 80% for nHA were denoted as NF-PLLA/nHA-30, NF-PLLA/nHA-50, and NF-PLLA/nHA-80, respectively.

For the preparation of PLLA scaffold without nanofibrous structure, a single solvent of dioxane was used to dissolve PLLA. The other procedures were the same as those for the preparation of NF-PLLA scaffold.

Characterizations

Morphology Observation. The surface morphologies of PLLA, NF-PLLA, and NF-PLLA/nHA scaffolds were observed by scanning electron microscopy (SEM, PHILIPS XL-30ESEM) with an acceleration voltage of 20.0 kV. Samples were cut to 1 mm in height, mounted on a copper stage, and spattered a gold layer before observation.

Specific Surface Area Test. The BET surface areas of various PLLA-based scaffolds were measured by N_2-adsorption experiments at liquid nitrogen temperature using the Brunauer-Emmett-Teller (BET) Analyzer (TriStar 3000, Micromeritics, USA). All samples were degassed at 60°C for 10 h before measurement.

Compression Test. The compressive property of the different PLLA-based scaffolds (8 mm in diameter and 10 mm in height) was measured on a universal material testing machine (BT1-FB005TN.D14, Zwick, Germany) at a crosshead speed of 1 mmmin^{-1}. The initial linear modulus on the stress–strain curves were defined as the compressive modulus.

Thermal Properties. The thermal analysis of various PLLA-based scaffolds were performed by differential scanning calorimetric (DSC, NETZSCH DSC 204F1 Phoenix, Germany) in a temperature range from 0 to 250°C with a heating rate of 10°C min^{-1}.

The degree of crystallization (X_c) was calculated according to the eq. (1):

$$X_c = (\Delta H_m / \Delta H_m^0) \times 100\% \quad (1)$$

ΔH_m is the heat of fusion, ΔH_m^0 is the heat fusion of 93.6 J g^{-1} for 100% crystalline PLLA.[21]

***In Vitro* Degradation.** Scaffolds of 8 mm × 5 mm (diameter × height) were used for *in vitro* degradation studies. Prior to incubation in phosphate buffered saline (PBS, pH = 7.4), samples were prewetted by a 1 : 1 (v/v) ethanol : PBS mixture solution. After being rinsed with PBS for four times (30 min each), the wetted scaffolds were immersed into 5 mL PBS and statically incubated at 37°C for various time periods up to 42 days. PBS solution was refreshed every 3 days. At each designed time point up to 6 weeks, three paralleled samples were removed from the solution, washed gently with distilled water four times (1 h each), and dried at vacuum for 48 h. The degradation was evaluated by the mass remaining percentage of scaffolds according to the equation of $M_{r,\ t}\% = W_t/W_0 \times 100\%$, where $M_{r,\ t}\%$ represented for the mass remaining percentage of scaffolds at the time of t, and W_t was for the residue weight of scaffolds at the time of t and W_0 was for the original weight of scaffolds before degradation.

Protein Adsorption. Scaffolds of 8 mm × 1 mm (diameter × height) were cut for the protein adsorption studies. Samples were prewetted with ethanol/PBS mixture (1 : 1, v/v), followed by thoroughly washed with PBS. The wetted scaffolds were soaked in a 5 mgmL^{-1} BSA solution in PBS at 37°C with a gentle shaking of 25 rpm for 4 h, followed by thrice washed in PBS to remove the free and loosely adsorbed proteins. The amount of protein adsorbed to the scaffolds was quantified by MicroBCA assay.[22]

Cells Culture. The viability of bone mesenchymal stem cell (BMSC) on the scaffolds was characterized by MTT (3-[4,5-dimethylthiazol-2-yl]-2,5-diphenyl-tetrazolium bromide) assay. Briefly, various PLLA-based scaffolds were cut into 5 mm × 2 mm (diameter × height) and placed into a 96-well plate after sterilization with 75% alcohol and thoroughly rinsed with PBS. Confluent

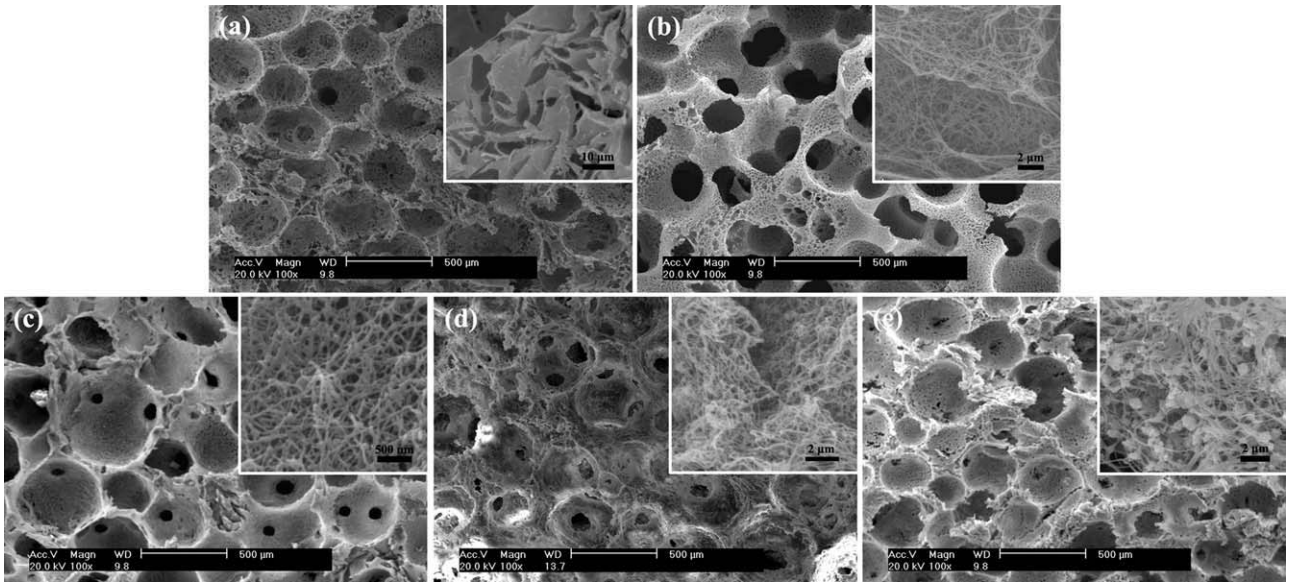

Figure 1. SEM micrographs of various PLLA-based porous scaffolds. (a) PLLA; (b) NF-PLLA; (c) NF-PLLA/nHA-30; (d) NF-PLLA/nHA-50; (e) NF-PLLA/nHA-80.

BMSC (Passage 3) were dissociated with 0.25% trypsin–EDTA (GIBCO) and resuspended in the L-DMEM (GIBCO) at a concentration of $\sim 5 \times 10^5$ cells mL^{-1}. A 100 μL cells suspension was injected to each well and incubated at 37°C under 5% CO_2 for 4 h. Subsequently, the scaffolds were transferred to another 96-well plate with fresh 100 μL L-DMED supplemented with 10% fetal bovine serum (FBS, GIBCO). After culturing for additional periods of 1, 3, 5, 7 days, 20 μL MTT solutions (5 $mgmL^{-1}$) were added to each well and incubated for another 4 h. The supernatant was discarded and the formazan crystals were dissolved by adding 100 μL of DMSO solution. The plates were kept at room temperature for 10 min, and then the optical density of each well was recorded at 490 nm using an automatic enzyme scanner (MK3, Labsystem Company, Finland).

The cells' morphology in the scaffolds at 7 days was also observed by SEM. Briefly, the PLLA-based scaffolds loaded with cells were gently rinsed with PBS thrice (10 min each), fixed in 2.5% (v/v) glutaraldehyde/PBS solution for 1 h at 4°C, and rinsed with PBS for another three times. After being dehydrated by incubation in a series of alcohol concentration (50, 60, 70, 80, 90, 95, and 100%) for 15 min, respectively, samples were mounted and coated with gold layer for SEM observation.

Statistical Analysis. All experimental data were expressed at means ± standard deviation (S.D.) by three tests. To test the significance of observed differences between the studies between the study groups, Student's t test was applied. A value of $P < 0.05$ was considered to be statistically significant.

RESULTS AND DISCUSSION

Morphology Observation

The surface morphologies of different PLLA-based scaffolds were observed by SEM, as shown in Figure 1. All the scaffolds exhibited interconnected porous structure with a macropore diameter of 300–450 μm that was generated from the paraffin porogens. A platelet structure was observed on the macropore wall of PLLA scaffold [Figure 1(a)], as opposed to the nanofibrous network ranging from 50 to 500 nm in bundle diameter for NF-PLLA scaffold [Figure 1(b)]. After incorporating nHA into NF-PLLA scaffold, the macropore surface became more compact, as shown in the images in low magnitude of Figure 1(c–e). From the images with higher magnification, it was observed that the nHA particles embedded among the nanofibers bundles. At a lower nHA content of 30%, the nHA particles uniformly deposit on the surface of the nanofibers bundles without visible aggregation phenomenon [Figure 1(c)]. With the increase of nHA content, especially for NF-PLLA/nHA-80, the nHA particles slightly aggregated to be larger particles and embedded in the gap of the nanofibers except the surface deposition because nanoparticles tended to spontaneously agglomerate at a high concentration for their large ratio surface energy.[23]

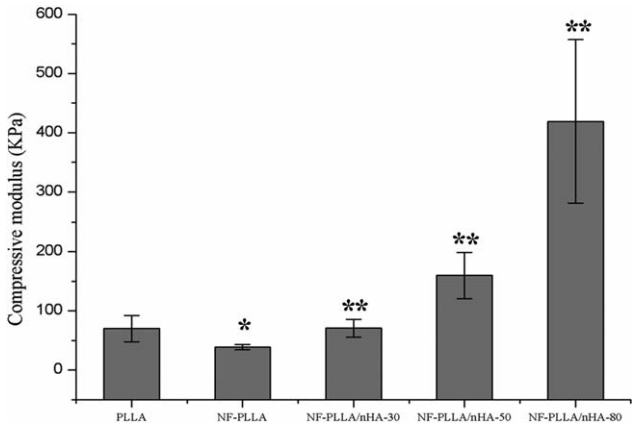

Figure 2. Compressive modulus of various PLLA-based scaffolds. Error bars represent means ± S.D., $n = 5$. Significant difference between NF-PLLA scaffold and PLLA scaffold ($^*P < 0.05$); Significant difference between NF-PLLA/nHA scaffolds and NF-PLLA scaffold ($^{**}P < 0.05$).

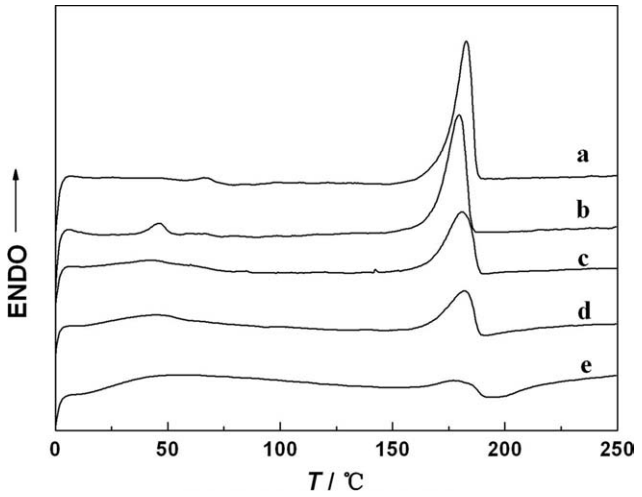

Figure 3. First-heating DSC curves of various PLLA based scaffolds. (a) PLLA; (b) NF-PLLA; (c) NF-PLLA/nHA-30; (d) NF-PLLA/nHA-50; (e) NF-PLLA/nHA-80.

However, the introduced nHA showed no obvious effect on the nanofibrous structure of NF-PLLA, which might act as the mechanical supporting points for improving the mechanical property of the composite scaffold.[24] To further illustrate the different surface morphologies for these PLLA-based scaffolds, their specific surface areas were measured to be 2.79, 34.06, 38.15, 44.38, and 53.19 $m^2\ g^{-1}$ for PLLA, NF-PLLA, NF-PLLA/nHA-30, NF-PLLA/nHA-50, and NF-PLLA/nHA-80 scaffolds, respectively. It showed that fabricating nanofibrous structure or incorporating nHA could increase the specific surface area of PLLA scaffold. Furthermore, the specific surface area increased with the increase of nHA content in the composite scaffold, due to the small particle size (55–60 nm in diameter) of nHA.

Mechanical Property

The compressive moduli of various PLLA-based scaffolds were shown in Figure 2. PLLA scaffold with platelet walls exhibited a compressive modulus of 70 ± 21 kPa, which was lower than the reported value from references ascribing to the high porosity (>90%, data not shown) and the relative lower matrix concentration (4%, w/v).[25] In contrast, NF-PLLA scaffold with nanofibrous network presented an even lower value of 39 ± 5 KPa. That was because nanofibrous scaffold lacked of mechanical supporting points between the nanofibers and would be likely to collapse by force.[20] However, the mechanical property was significantly improved by incorporating nHA into NF-PLLA scaffold. Furthermore, the compressive modulus of NF-PLLA/nHA scaffold increased by enhancing the nHA content. At a weight percentage of 80% for nHA, the compressive modulus of the composite scaffold reached 419 ± 110 KPa, which was about 10 times as that of NF-PLLA scaffold. It might be the reason that nHA, deposited on the nanofibers, acted as the mechanical support points under compression and could consume some external force, such that the compression performance of the composite scaffold was improved.[26] In particular, for NF-PLLA/nHA-80, besides the contribution of nHA depositing on the nanofibers surface, the formation of nHA aggregates that were wrapped by the PLLA nanofibers would make the matrix more robust. These results showed that the introduction of nHA could effectively improve the mechanical property of NF-PLLA scaffold, which was proportional to the nHA content in the composite scaffold.

DSC Analysis

Figure 3 shows the first heating DSC patterns of various PLLA-based scaffolds. The corresponding thermal properties data were summarized in Table I. NF-PLLA scaffold showed a glass transition temperature (T_g) of 46.0°C, a melting point (T_m) of 179.8°C, and a crystallinity (X_c) of 64.2% respectively, which were lower than those of 66.0°C (T_g), 182.8°C (T_m), and 69.0% (X_c) for PLLA scaffold. These differences between PLLA and NF-PLLA scaffolds might be attributed to their different phase separation process. For NF-PLLA scaffold, PLLA molecules dissolved in a mixture solvent of dioxane and pyridine was more likely to be separated out by cooling, leading to the formation of imperfect crystals that was responsible for the lower T_g, T_m, and X_c as well as the broader melting peak.[27]

After blending nHA, with increasing the nHA content, the X_c of the composite scaffold was getting smaller and smaller, i.e., 60.3, 58.3, and 56.4% for NF-PLLA/nHA-30, NF-PLLA/nHA-50, and NF-PLLA/nHA-80, respectively. The melting peak also became broader and broader, which almost disappeared when the nHA content was raised to 80% (wt). The decrease of X_c should be owed to the increasing defects of PLLA crystals by raising the content of nHA that might act as the nucleating agent during the phase separation.[22] However, the T_m value displayed no regular changes with the nHA content, but presented a broader melting peak at higher nHA content. The broadening of the melting peak for NF-PLLA/nHA scaffolds with increasing the nHA content should be resulted from the decreasing crystallinity of NF-PLLA in this composite. Generally, for crystalline polymers, a low crystallinity would lead to a broad melting

Table I. Thermal Properties of Various PLLA-Based Porous Scaffolds

Scaffold	T_g (°C)	T_m (°C)	ΔH_m (J g^{-1})	X_c (%)	$Y^*_{1/2}$ (°C)
PLLA	66.0	182.8	64.6	69.0	8.6
NF-PLLA	46.0	179.8	60.1	64.2	9.9
NF-PLLA/nHA-30	-	180.7	60.3	64.4	13.5
NF-PLLA/nHA-50	-	182.0	58.3	62.3	13.6
NF-PLLA/nHA-80	-	178.8	56.4	60.3	19.7

$Y^*_{1/2}$: peak width at half height.

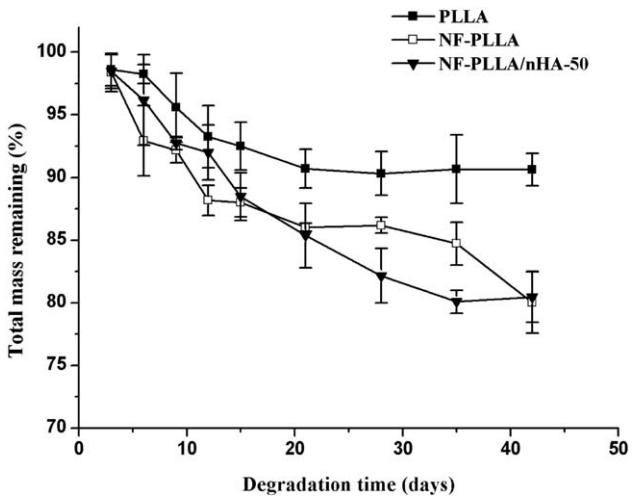

Figure 4. Changes in total mass remaining percentage of various PLLA-based scaffolds during the *in vitro* degradation in PBS at 37°C. Error bars represent means ± S.D., $n = 3$. All samples are different from one another at $P < 0.05$.

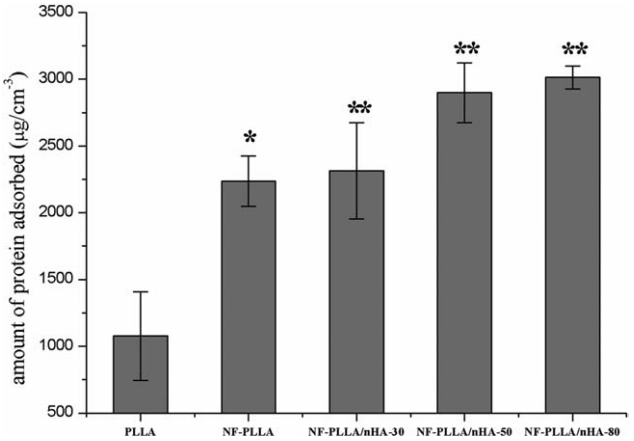

Figure 5. Adsorption of BSA on the surface of various PLLA-based scaffolds. Error bars represent means ± S.D., $n = 3$. Significant difference between NF-PLLA scaffold and PLLA scaffold ($^*P < 0.05$); Significant difference between NF-PLLA/nHA scaffolds and NF-PLLA scaffold ($^{**}P < 0.05$).

peak.[28] These results suggested that the presence and amount of nHA in the composite matrix had a significant effect on the thermal properties of NF-PLLA scaffold.

In Vitro Degradation

The total mass remaining percentage of various PLLA-based scaffolds during the *in vitro* degradation was shown in Figure 4. During the whole incubation period, NF-PLLA and NF-PLLA/nHA-50 scaffolds showed a faster degradation rate than PLLA scaffold. At 42 days, there were 80.0 and 80.4% in mass remaining for NF-PLLA and NF-PLLA/nHA-50 scaffolds, respectively in comparison to 91.3% for PLLA scaffold. It should be owed to the higher specific surface area and lower crystallinity for NF-PLLA and NF-PLLA/nHA-50 scaffolds that provided more opportunities for water molecules attacking the ester bonds on PLLA molecule chains, and hereby induced to the faster hydrolysis of the matrix.[29] NF-PLLA/nHA-50 scaffolds showed a similar degradation rate with NF-PLLA scaffold in spite of the presence of hydrophilic nHA and a lower crystallinity. It implied that the specific surface area was the predominant factor contributing to the rapid degradation of PLLA-based matrix.

Protein Adsorption

The interaction between cells and matrix was mediated by the proteins that adsorbed on the surface of the matrix; hence, the protein adsorption behavior is an important parameter to evaluate the tissue engineering scaffolds.[30] Figure 5 illustrates the adsorption of BSA on the surface of various PLLA-based scaffolds. NF-PLLA scaffold showed a BSA adsorption ability of 2237 ± 188 μg cm^{-3} that was over twice as that of 1077 ± 332 μg cm^{-3} for PLLA scaffold due to the much larger specific surface area than PLLA scaffold. After incorporating nHA, the amount of BSA adsorbed on the surface of NF-PLLA/nHA scaffold was further enhanced by increasing the nHA content. It was possible that the blended nHA was in favor of the BSA adsorption because of its hydrophilicity and the increasing specific surface area with the nHA content for NF-PLLA/nHA scaffolds since the protein adsorption can be influenced by topology and chemical composition of the incorporated bone-like mineral component.[31,32]

Cells Viability

The BMSC viability in different PLLA-based scaffolds for *in vitro* culture up to 7 days were evaluated by MTT analysis, as shown in Figure 6. It is known that the cell number was positively relevant to the absorbance optical density value that can indirectly represent cells viability.[33] With the increase of cultivation time, the amount of cells on all kinds of scaffolds increased, indicating that BMSC could grow on all these PLLA-based scaffolds. However, the cell proliferation rate on NF-PLLA

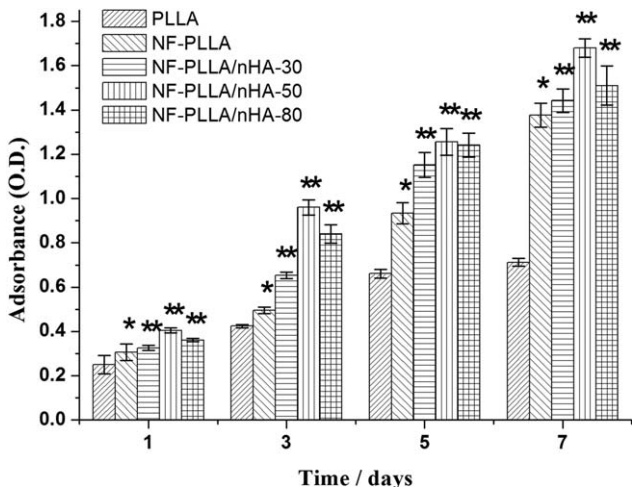

Figure 6. MTT assays of BMSCs seeding on various PLLA-based scaffolds during the observation periods. Error bars represent means ± S.D., $n = 3$. Significant difference between NF-PLLA scaffold and PLLA scaffold ($^*P < 0.05$); Significant difference between NF-PLLA/nHA scaffolds and NF-PLLA scaffold ($^{**}P < 0.05$).

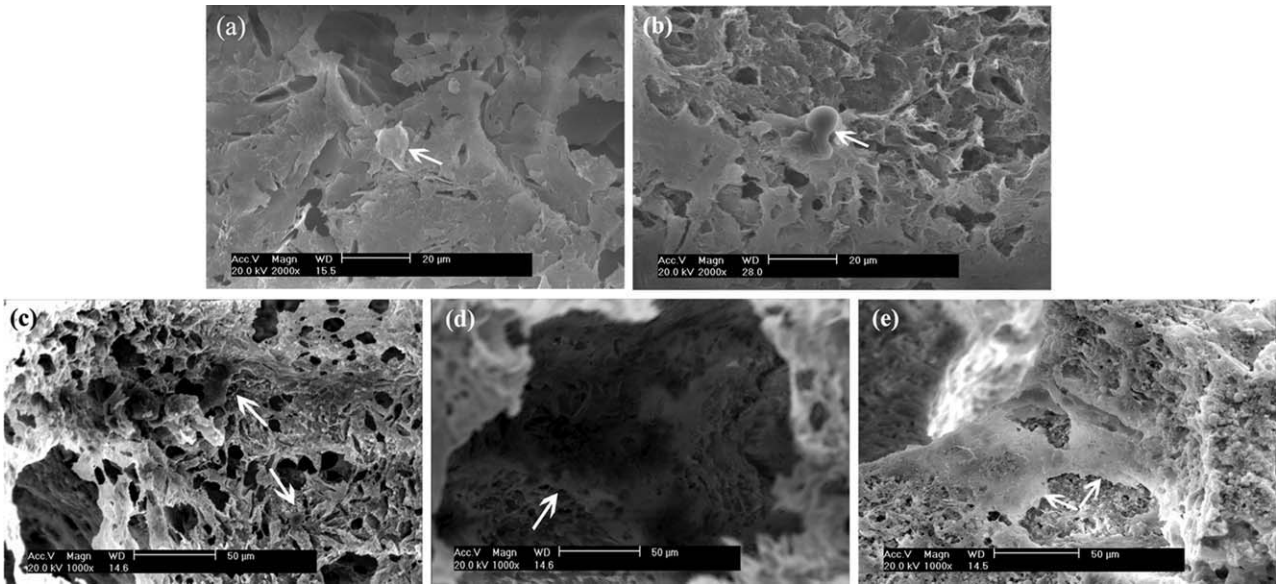

Figure 7. SEM micrographs of BMSCs seeding on the tested PLLA based scaffolds after 7-days cultivation. (a) PLLA scaffold; (b) NF-PLLA scaffold; (c) NF-PLLA/nHA-30 scaffold; (d) NF-PLLA/nHA-50 scaffold; (e) NF-PLLA/nHA-80 scaffold. Arrow: BMSCs.

scaffold was significantly higher than that on PLLA scaffold due to the nanofibrous structure and much larger specific surface area of nanofibrous scaffolds that had been proved to facilitate cell attachment and growth.[14] By incorporating nHA particles, the BMSC proliferation rate got further increased in comparison to NF-PLLA scaffold, and NF-PLLA/nHA-50 exhibited the fastest cell growth during the whole incubation period among the three NF-PLLA/nHA samples. It suggested that the presence of nHA was advantageous to the increase of the BMSC viability. It had been revealed that the calcium in HA might play a role in unfolding the adhesion molecules, which in turn expose the cell adhesive epitopes recognized by specific cell surface integrins.[34] The highest cell viability appeared for the composite scaffold with medium nHA content, i.e., NF-PLLA/nHA-50, suggesting that both nanofibrous structure and nHA particles could simultaneously influence the cell growth, but here an optimal nHA composition for NF-PLLA/nHA scaffolds was 50% in weight percentage. Figure 7 shows the BMSC morphologies after culture for 7 days in PLLA, NF-PLLA, and NF-PLLA/nHA scaffolds. The cells loosely adhered on the surface of PLLA scaffold and showed a spherical shape with a proximate size of 10 μm in diameter [Figure 7(a)]. By contrast, the cells on NF-PLLA scaffold presented a much tighter attachment with a stretched morphology of about 20 μm in length [Figure 7(b)]. After incorporating nHA particles, especially for NF-PLLA/nHA-50 and NF-PLLA/nHA-80 scaffolds, the cells completely stretched on the scaffold surface and displayed a much larger size of over 50 μm [Figure 7(d, e)]. The size of cells on NF-PLLA/nHA-50 scaffold even reached about 100 μm, showing the largest stretched morphology among all the PLLA-based scaffold samples. It indicated that the nanofibrous structure of PLLA was beneficial to the BMSC attachment, and the introduction of nHA could speed up the further growth of BMSC. The best BMSC viability was obtained on NF-PLLA/nHA-50 scaffold, which was in consistent with the results from MTT assay.

CONCLUSIONS

NF-PLLA/nHA composite scaffold with interconnected macropore was created by a TIPS technique in the presence of nHA particles. This scaffold showed 3D nanofibrous structure with a bundle diameter of 50–500 nm that mimicked the fibrillar collagen in natural ECM. The incorporation of nHA increased the specific surface area and had no effect on the nanofibrous structure of NF-PLLA scaffold, but distinctively improved the compressive modulus. The introduced nHA also played a significant influence on the thermal properties of NF-PLLA scaffold. The T_m and X_c of NF-PLLA/nHA scaffolds decreased with the increase of nHA content. Additionally, NF-PLLA and NF-PLLA/nHA scaffolds exhibited a faster degradation rate and larger BSA adsorption than PLLA scaffold due to their much larger specific surface area. Among these PLLA-based scaffolds, NF-PLLA/nHA-50 showed the highest cell viability ascribing to the nanofibrous structure of PLLA and optimal nHA composition. This strengthened NF-PLLA/nHA composite scaffold would be a promising biomimetic scaffold for bone tissue engineering.

ACKNOWLEDGMENTS

The authors are thankful for financial support from the National High Technology Research and Development Program of China (863 Program) (No. 2007AA09Z440) and the National Natural Science Foundation of China (No. 30900296).

REFERENCES

1. Ma, P. X. *Adv. Drug Deliv. Rev.* **2008,** *60*, 184.
2. Shin, H.; Jo, S.; Mikos, A. G. *Biomaterials* **2003,** *24*, 4353.
3. Hay, E. D. *J. Cell Biol.* **1981,** *91*, 205.
4. Ma, P. X.; Zhang, R. Y. *J. Biomed. Mater. Res. A* **1999,** *46*, 60.

5. Liao, S.; Chan, C. K.; Ramakrishna, S. *Mater. Sci. Eng. C* **2008,** *28*, 1189.
6. Liu, X. H.; Smith, L. A.; Hu, J.; Ma, P. X. *Biomaterials* **2009,** *30*, 2252.
7. Wei, G. B.; Ma, P. X. *Adv. Funct. Mater.* **2008,** *18*, 3568.
8. Smith, I. O.; Liu, X. H.; Smith, L. A.; Ma, P. X. *Nanomed. Nanobiotechnol.* **2009,** *1*, 226.
9. Peng, F.; Yu, X. H.; Wei, M. *Acta Biomater.* **2011,** *7*, 2585.
10. Hu, J.; Sun, X.; Ma, H. Y.; Xie, C. Q.; Chen, Y. E.; Ma, P. X. *Biomaterials* **2010,** *31*, 7971.
11. Park, J. E.; Todo, M. *J. Mater. Sci. Mater. M.* **2011,** *22*, 1171.
12. He, L. M.; Zhang, Y. Q.; Zeng, X.; Quan, D. P.; Liao, S.; Zeng, Y. S.; Lu, J.; Ramakrishna, S. *Polymer* **2009,** *50*, 4128.
13. Liu, X. H.; Ma, P. X. *Biomaterials* **2010,** *31*, 259.
14. Smith, L. A.; Liu, X. H.; Hu, J.; Ma, P. X. *Biomaterials* **2009,** *30*, 2516.
15. Wei, G.; Ma, P. X. *Biomaterials* **2004,** *25*, 4749.
16. Liu, X. H.; Smith, L. A.; Hu, J.; Ma, P. X. *Biomaterials* **2009,** *30*, 2252.
17. Hench, L. L. *J. Am. Ceram. Soc.* **1998,** *81*, 1705.
18. Ng, A. M.; Tan, K. K.; Phang, M. Y.; Aziyati, O.; Tan, G. H.; Isa, M. R.; Aminuddin, B. S.; Naseem, M.; Fauziah, O.; Ruszymah, B. H. *J. Biomed. Mater. Res. A* **2008,** 85A, 301.
19. Wei, K.; Wang, Y. J.; Lai, C.; Ning, C. Y.; Wu, D. X.; Wu, G.; Zhao, N. R.; Chen, X. F.; Ye, J. D. *Mater. Lett.* **2005,** *59*, 220.
20. Chen, V. J.; Ma, P. X. *Biomaterials* **2004,** *25*, 2065.
21. Lee, I. C.; Cheng, L. P.; Young, T. H. *J. Biomed. Mater. Res. A* **2006,** *76A*, 842.
22. Wei, G. B.; Ma, P. X. *Biomaterials* **2004,** *25*, 4749.
23. Fang, L.; Leng, Y.; Gao, P. *Biomaterials* **2006,** *27*, 3701.
24. Kane, R. J.; Roeder, R. K. *J. Mech. Behav. Biomed.* **2012,** *7*, 41.
25. Ma, P. X.; Choi, J. W. *Tissue Eng.* **2001,** *7*, 23.
26. Hayati, A. N.; Hosseinalipour, S. M.; Rezaie, H. R.; Shokrgozar, M. A. *Mater. Sci. Eng. C* **2012,** *32*, 416.
27. Zhao, J. H.; Han, W. Q.; Chen, H. D.; Tu, M.; Zeng, R.; Shi, Y. F.; Cha, Z. G.; Zhou, C. R. *Carbohydr. Polym.* **2011,** *83*, 1541.
28. Tsuji, H.; Kawashima, Y.; Takikawa, H. *J. Polym. Sci. B Polym. Phys.* **2007,** *45*, 2167.
29. Chen, V. J.; Ma, P. X. *Biomaterials* **2006,** *27*, 3708.
30. Woo, K. M.; Chen, V. J.; Ma, P. X. *J. Biomed. Mater. Res. A*, **2003,** *67A*, 531.
31. Talal, A.; Waheed, N.; Al-Masri, M.; McKay, I. J.; Tanner, K. E.; Hughes, F. J. *J. Dent.* **2009,** *37*, 820.
32. Woo, K. M.; Seo, J.; Zhang, R.; Ma, P. X. *Biomaterials* **2007,** *28*, 2622.
33. Brunot, C.; Grosgogeat, B.; Picart, C.; Lagneau, C.; Jaffrezic-Renault, N.; Ponsonnet, L. *Dent. Mater.* **2008,** *24*, 1025.
34. Webster, T. J.; Schadler, L. S.; Siegel, R. W.; Bizios, R. *Tissue Eng.* **2001,** *7*, 291.